Received June 13, 2019, accepted June 26, 2019, date of publication July 2, 2019, date of current version August 16, 2019.

Digital Object Identifier 10.1109/ACCESS.2019.2926353

Cramér–Rao Lower Bound Analysis for Stochastic Model Based Target Parameter Estimation in Multistatic Passive Radar With Direct-Path Interference

JING TONG, HUANG GAOMING, TIAN WEI, AND PENG HUAFU
College of Electronic Engineering, Naval University of Engineering, Wuhan 430033, China

Corresponding author: Huang Gaoming (hgaom_paper@163.com)

This work was supported in part by the National Natural Science Foundation of China under Grant 61803379, and in part by the China Postdoctoral Science Foundation under Grant 2017M613370 and Grant 2018T111129.

ABSTRACT This paper addresses the problem of Cramér–Rao lower bound (CRLB) analysis for joint target location and velocity estimation in a multistatic passive radar system comprised of multiple noncooperative illuminators of opportunity (IOs) and multiple geographically separated receivers. Unlike other existing studies, special attention in this paper is paid to a more ubiquitous scenario, in which no reference channel exists in receiver networks. Besides, the situation where the measurements collected at the receivers are contaminated by the interference directly illuminated from the IOs is taken into account. Namely, each receive station simultaneously obtains direct-path interference (DPI) from all the IOs and echo signals reflected by the target. Furthermore, the IO waveform is modeled as a stochastic process in which samples of the unknown IO waveform are treated as a complex Gaussian sequence. Finally, the effects of multipath clutter on the signal model and CRLB are well analyzed. The numerical results are provided to prove that the joint CRLB is not only a function of the signal-to-noise ratio (SNR), DPI-to-noise ratio (DNR), and clutter-to-noise ratio (CNR) but also associated with both IO waveform parameters and relative geographical distribution of the system.

INDEX TERMS Passive radar, passive multistatic radar, Cramér–Rao lower bound, direct-path interference (DPI), stochastic process.

I. INTRODUCTION

Passive radar, also known as passive coherent location (PCL), utilizes existing noncooperative illuminators of opportunity (IOs) rather its own dedicated transmitter for target detection and estimation [1]–[6]. Such radars have a number of advantages compared with their conventional active counterparts. First, passive radar is much smaller, utmost economical, and easily designed since no additional transmitters are required. Additionally, electromagnetic spectrum resources are effectively saved. Second, the receiver is able to operate covertly, which greatly reduces the detectability and improves the viability of the system. Furthermore, the target can be viewed from different perspectives in bistatic or multistatic configuration, which provides the system with advantages of anti-stealth and anti-low altitude penetration. However, these superiorities are obtained at the expense of extensive computation, complex processing, and complicated algorithm. Besides, unlike active radar that uses cooperative transmitter and dedicated signal designed for target detection and estimation, prior knowledge of IO waveform is generally unknown to the receiver in passive radar. Whereby, the characteristics of these waveforms must be analyzed in essence. Hence, in recent years, many available IOs have been attracting intensive attention such as global positioning system (GPS) [7], digital video broadcasting-terrestrial (DVB-T) [8], [9], frequency modulation (FM) radio [10], [11], WiFi [12], and analogue TV (ATV) [13].

The Cramér–Rao lower bound (CRLB) is a predominant theoretical analysis tool for parameter estimation, which

The associate editor coordinating the review of this manuscript and approving it for publication was Abdel-Hamid Soliman.

specifies the minimum error variance of any unbiased estimator. Namely, it tells us the best that could be achieved. In passive radar systems, CRLB and some of its variations are frequently used for setting a lower bound of the parameter estimation under different scenarios, benchmarking the performance of a certain delay-Doppler estimator, evaluating the merits of different algorithms, and designing a transmitter selection scheme [14]–[26]. In [14], the ambiguity function (AF) and modified CRLBs (MCRLBs) for target range and velocity of the PCL system using universal mobile telecommunications system (UMTS) signal as the IO in both bistatic and monostatic configuration were calculated. Reference [15] extends the results in [14] from bistatic to a multistatic scenario with multiple IOs. Moreover, MCRLB for target estimation is deduced under both coherent and non-coherent modes, which indicates that the MCRLB expression relies on not only the IO waveform but also the relative geographic relation of the multistatic radar-target configuration. Reference [16] further extends the MCRLB on target position and velocity considering the line-of-sight (LOS) and non-LOS components of the echo signals reflected by a single target in a three-dimensional (3D) coordinate system. In [17], a more practical expression of CRLB is provided, which considers that the system may miss detection. Reference [18] calculates the CRLB of the target location and velocity on the assumption that IOs can be precisely estimated in a passive radar network, where the multiple transmitters and multiple receivers with single antenna are all widely distributed. It proves that the parameter estimation performance can be improved by increasing the number of transmitters or receivers. Similar to [15], the CRLB for joint target estimation in FM-based passive radar networks under both coherent and non-coherent cases is deduced in [19]. Based on [19], [20] is committed to a transmitter selection problem in the same sensor network using the coherent CRLB as the selection criteria. Furthermore, [21] and [22] also study the sensor selection problem based on CRLB. In particular, [21] studies how to optimally arrange receiver location, while [22] expounds a scheme to dynamically select IOs. Despite numerous research on CRLB has been carried out in the field of passive radar, whereas, most of those work is limited by a surge of factors in practice.

This paper completes a detailed investigation of CRLB for joint target location and velocity estimation in a more practical scenario. First, different from most existing research with the investigation of deterministic signal model, our CRLB analysis is carried out treating the IO waveform as a stochastic process [24], [27]–[29]. This is because, the waveform information of the IO signal cannot be completely acquired in many cases, but only its statistical distribution. Moreover, IOs transmitted with multiplexing techniques, such as orthogonal frequency division multiplexing (OFDM) signals, are widely deployed and quite appropriate for modeling as stochastic process in the light of the central limit theorem [30]. Therefore, modeling the IO signal as a stochastic process without any information of the waveform is quite reasonable and can be applied to more general scenarios in passive radar systems. Whereby, with reference to [24], an autoregressive process with known AR coefficient and noise variance is exploited to model the IO signal in this work.

Second, we expand the system structure in [24] and [29] to a multistatic configuration comprised of multiple IOs and multiple geographically separated receivers. It is noteworthy at this point that only single antenna is established in each receive station, namely, no additional antenna set to collect direct-path signals for reference, which is similar to the concept of active multiple-input multiple-output (MIMO) radar systems [28]. That is because, significant performance improvement can be obtained by increasing the number of IOs and receivers [18], [19]. More importantly, the conventional approach using reference channel is seriously affected by the signal-to-noise ratio (SNR) of the direct-path signal. However, in practical applications, reference signal with high SNR cannot be ideally obtained for many reasons, e.g., no LOS path existing between the IO and the receiver, which may significantly lead to detection performance degradation of the system [31]. The system model in this study can avoid this problem whilst offering advantages of spatial diversity and wider coverage to improve the detection and estimation performance. Third, we also consider the impacts of the direct-path signals enclosed in the target-path echoes due to the still existing direct-path interference (DPI) after some interference cancellation methods. In addition, signals obtained by all receivers can be centrally processed to take advantage of the correlations between all types of signals across receivers in this configuration, which is able to get better performance gains for detecting in practice [32].

Finally, the theoretical calculations are demonstrated by simulation results, and corresponding analysis is then given. It should be mentioned that [27] only provide the detection analysis in multistatic scenario with single IO, and no detailed research of CRLB on parameter estimation is provided. Taken all mentioned above, a more practical and adaptable problem model is studied in this paper, and related CRLB expression is derived, which is particularly worthy of academic investigation. To our knowledge, the specific study of the CRLB for stochastic model based joint target location and velocity estimation in multistatic passive radar with DPI is not yet gained. For greater clarity, the main contributions of this work are concluded as follows.

1) The signal model is formulated under the case where the multistatic configuration are composed of multiple IOs and receivers without reference channels, and the DPI is simultaneously considered.

2) We calculate the joint CRLB for target location and velocity estimation based on stochastic model under the foregoing scenario.

3) The effects of multipath clutter on the model and CRLB are analyzed in detail.

4) We have revealed that the CRLB depends on not only the IO waveform parameters and relative geometry between the target and the radar system, but also the value of SNR, DPI-to-noise ratio (DNR), and clutter-to-noise ration (CNR).

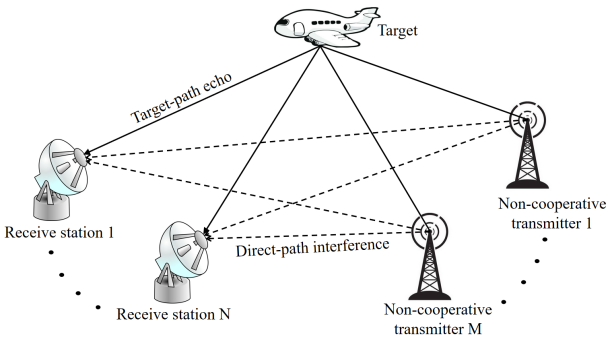

FIGURE 1. The passive radar system comprised of multiple IOs and multiple receive stations with DPI.

The rest of the paper is organized as follows. In Section 2, the collected signal model in the multistatic configuration considering the existence of DPI is given. In Section 3, we derive the expression of Fisher information matrix (FIM) for unknown target parameters, and then the CRLB of interest is given. Numerical simulations are presented in Section 4 to verify the theoretical derivation. Finally, Section 5 summarizes the results of this work and provides future directions of research.

II. SIGNAL MODEL

Fig. 1 displays the considered multistatic geometry. Consider a passive radar system involving M separated noncooperative transmitters, N distributed receivers, and one target located at a certain location and speed. For simplicity, the problem is analyzed in a two-dimensional plane. Without loss of generality, one can easily extend the results to a 3D scenario. Hence, the positions of the pth transmitter and qth receiver are denoted by $\mathbf{T}_p = [T_p^x, T_p^y]^T$ and $\mathbf{R}_q = [R_q^x, R_q^y]^T$, respectively. The target position and velocity states that are unknown to the receive networks are defined as $\mathbf{X}_t = [x, y]^T$ and $\mathbf{X}_v = [v_x, v_y]^T$, respectively. For the reason that the number of unknown parameters to be estimated will be increased as the number of targets increases, which can make the analysis more complicated, only one target is considered in this study. The case with multiple targets will be discussed in future work. In addition, although some suppression methods are taken to eliminate the direct-path signals contained in target echoes, the received measurements will be inevitably corrupted by the residual DPI. Let $y_q(t)$ be the signal received at the qth receiver. Hence,

$$y_q(t)=\sum_{p=1}^{M}\gamma_{pq}x_p(t-\tau_{pq}^d)+\sum_{p=1}^{M}\alpha_{pq}x_p(t-\tau_{pq}^t)e^{j2\pi f_{pq}t}+n_q(t), \tag{1}$$

where $p = 1, 2, \ldots, M, q = 1, 2, \ldots, N.x_p(t)$ is the unknown signal emitted by the pth IO, which has a duration of T_p seconds owing to the IO utilizing framed transmissions [24]. γ_{pq} and α_{pq} are complex channel coefficients according to the pqth direct-path and target echo-path, respectively. $n_q(t)$ is the additive zero-mean white Gaussian noise of the qth receiver with variance σ_q^2, which is assumed to be deterministic and known. The direct-path delay τ_{pq}^d, target-path delay τ_{pq}^t, and Doppler frequency f_{pq} of the pqth bistatic pair are defined as

$$\begin{aligned}\tau_{pq}^d &= \frac{\sqrt{(T_p^x-R_q^x)^2+(T_p^y-R_q^y)^2}}{c}\\ &= \frac{\|\mathbf{T}_p-\mathbf{R}_q\|_2}{c},\end{aligned} \tag{2}$$

$$\begin{aligned}\tau_{pq}^t &= \frac{\sqrt{(T_p^x-x)^2+(T_p^y-y)^2}+\sqrt{(R_q^x-x)^2+(R_q^y-y)^2}}{c}\\ &= \frac{\|\mathbf{T}_p-\mathbf{X}_t\|_2+\|\mathbf{R}_q-\mathbf{X}_t\|_2}{c},\end{aligned} \tag{3}$$

$$\begin{aligned}\lambda_p f_{pq} &= \frac{\left(T_p^x-x\right)v_x+\left(T_p^y-y\right)v_y}{\|\mathbf{T}_p-\mathbf{X}_t\|_2}\\ &\quad+\frac{\left(R_q^x-x\right)v_x+\left(R_q^y-y\right)v_y}{\|\mathbf{R}_q-\mathbf{X}_t\|_2}\\ &= \frac{(\mathbf{T}_p-\mathbf{X}_t)^{\mathrm{T}}\mathbf{X}_v}{\|\mathbf{T}_p-\mathbf{X}_t\|_2}+\frac{(\mathbf{R}_q-\mathbf{X}_t)^{\mathrm{T}}\mathbf{X}_v}{\|\mathbf{R}_q-\mathbf{X}_t\|_2},\end{aligned} \tag{4}$$

where c is the speed of light, λ_p is the carrier wavelength of the pth IO signal, and $\|\cdot\|_2$ represents the Euclidean distance between two vectors. It is worth mentioning that the above signal model is based on the assumption that the signals from different IOs are able to be separated with some methods.

As with literature [24], the IO coordinates are assumed to be entirely known. Whereas, due to multiple IOs locating at different positions in this multistatic geometry, the direct-path delays cannot be all compensated for by one of them. Compared with [24] that derives the CRLB based on the frequency domain representation of the received signal, time domain representation is employed in our derivation. Let the received signal $y_q(t)$ be sampled with sampling points N_s, where the observation duration is T_o and the sampling interval is T_s, i.e., $T_o = T_sN_s$. Thus, the digitized expression of $y_q(t)$ after a series of equivalent transformation is expressed as [29], [31]

$$\mathbf{y}_q=\sum_{p=1}^{M}\gamma_{pq}\mathbf{A}(\tau_{pq}^d)\mathbf{x}_p+\sum_{p=1}^{M}\alpha_{pq}\mathbf{B}(\tau_{pq}^t,f_{pq})\mathbf{x}_p+\mathbf{n}_q, \tag{5}$$

where $\mathbf{x}_p$ and $\mathbf{n}_q$ are the vectors composed of sampling points of $x_p(t)$ and $n_q(t)$, respectively. In particular, $\mathbf{n}_q$ is a zero-mean Gaussian noise sequence with covariance matrix $\mathbf{U}_{n_q}$. $\mathbf{A}(\tau_{pq}^d)$ is the delay operator for DPI, and $\mathbf{B}(\tau_{pq}^t, f_{pq})$ is the delay-Doppler operator for target-path signal, which are denoted as

$$\mathbf{A}(\tau_{pq}^d) = \mathbf{F}^H\boldsymbol{\Omega}(\tau_{pq}^d)\mathbf{F}, \tag{6}$$

$$\mathbf{B}(\tau_{pq}^t, f_{pq}) = \boldsymbol{\varphi}(f_{pq})\mathbf{F}^H\boldsymbol{\Omega}(\tau_{pq}^t)\mathbf{F}, \tag{7}$$

where $\mathbf{F}$ is the discrete Fourier transform (DFT) matrix with entries $[\mathbf{F}]_{m,n} = \exp[-j2\pi(m-1)(n-1)/N_s]$, and

$m, n = 1, 2, \ldots, N_s$. $\boldsymbol{\varphi}(f_{pq})$, a diagonal matrix with diagonal entries $[\boldsymbol{\varphi}(f_{pq})]_{m,m} = \exp[j2\pi(m-1)f_{pq}T_s]$, represents the phase shift of the transmitted signal caused by the Doppler frequency. $\boldsymbol{\Omega}(\tau_{pq}^d)$ and $\boldsymbol{\Omega}(\tau_{pq}^t)$ indicate the phase shift in the frequency domain due to the direct-path delay and target-path delay of the pqth bistatic pair, both of which are also diagonal matrices with diagonal entries calculated by $[\boldsymbol{\Omega}(\tau_{pq}^d)]_{m,m} = \exp[-j2\pi(m-1)\tau_{pq}^d/T_sN_s]$ and $[\boldsymbol{\Omega}(\tau_{pq}^t)]_{m,m} = \exp[-j2\pi(m-1)\tau_{pq}^t/T_sN_s]$, respectively.

Most existing research studies the target detection and estimation problem based on deterministic signal with unknown parameters. However, in most cases, the receiver networks know nothing about the specific structure and modulation of the IOs likely used, especially when the passive radar system needs to be rapidly deployed in unfamiliar areas. Hence, a universal solution for this problem is supposed to be proposed. Modeling the IO signal as a stochastic process is reasonable. First, OFDM modulation technology is widely used in modern communication for its excellent performance, which can be almost treated as a Gaussian process by the central limit theorem. Second, correlations between the sampled waveforms can be effectively exploited to improve the detection and estimation performance. Finally, Even if the actual IO signal mismatches the model, a desired result can be still obtained with certain algorithm [29]. Therefore, CRLB based on a stochastic process model is necessary to be analyzed. Here, the AR process is used to model the IO signal, where $\mathbf{x}_p$ is a zero-mean Gaussian distributed sequence with covariance $\mathbf{U}_{x_p}$ expressed as

$$[\mathbf{U}_{x_p}]_{m,n} = \frac{\sigma_{c_p}^2(-\rho_p)^{|m-n|}}{1-|\rho_p|^2}, \tag{8}$$

where $m, n = 1, 2, \ldots, N_{c_p}$. $N_{c_p} = T_p/T_s + 1$ indicates the number of $\mathbf{x}_p$ samples. $\sigma_{c_p}^2$ represents the noise variance in AR process, and ρ_p denotes the AR coefficient that reflects the correlation between the contiguous samples of $\mathbf{x}_p$ in time domain. It should be noted that $\sigma_{c_p}^2$ and ρ_p are deterministic known, which can be determined by fitting the AR model with some methods, e.g., recursive prediction error (RPE) [33], maximum likelihood (ML) [34], and least squares (LS) [35]. The actual parameters of the IO signal could affect its physical model, and then, the characteristics of the signal samples, which may determine the parameters in AR model. However, the estimation accuracy of these parameters is mainly dependent on sampled data, e.g., the number of the samples.

III. DERIVATION OF CRLB

This CRLB analysis offers a performance benchmark for joint estimation of the unknown target parameters. Let $\mathbf{y} = [\mathbf{y}_1^T, \mathbf{y}_2^T, \cdots \mathbf{y}_N^T]^T$ be the measurements collected at N receivers, where $\mathbf{y}_q = \{y_q(0), y_q(T_s), \cdots y_q[(N_s-1)T_s]\}^T$. Since receivers are widely separated, it is reasonable to suppose that $\mathbf{y}_q$ are mutually independent for each other. Obviously, $\mathbf{y}$ is complex zero-mean Gaussian distributed with covariance $\mathbf{U}_y$, where

$$\mathbf{U}_y = E[\mathbf{y}\mathbf{y}^H] = E\begin{bmatrix} \mathbf{y}_1\mathbf{y}_1^H & \cdots & \mathbf{y}_1\mathbf{y}_N^H \\ \vdots & \ddots & \vdots \\ \mathbf{y}_N\mathbf{y}_1^H & \cdots & \mathbf{y}_N\mathbf{y}_N^H \end{bmatrix}. \tag{9}$$

For convenience of calculation, we rewrite formula (9) in a more simplified form as [27]

$$\begin{aligned}\mathbf{U}_y = \sum_{p=1}^{M} \{&\mathbf{A}_p[(\boldsymbol{\gamma}_p\boldsymbol{\gamma}_p^H)\otimes\mathbf{U}_{x_p}]\mathbf{A}_p^H + \mathbf{B}_p[(\boldsymbol{\alpha}_p\boldsymbol{\alpha}_p^H)\otimes\mathbf{U}_{x_p}]\mathbf{B}_p^H \\ &+\mathbf{B}_p[(\boldsymbol{\alpha}_p\boldsymbol{\gamma}_p^H)\otimes\mathbf{U}_{x_p}]\mathbf{A}_p^H + \mathbf{A}_p[(\boldsymbol{\gamma}_p\boldsymbol{\alpha}_p^H)\otimes\mathbf{U}_{x_p}]\mathbf{B}_p^H\} + \mathbf{U}_v,\end{aligned} \tag{10}$$

where $\boldsymbol{\gamma}_p = [\gamma_{p1}, \gamma_{p2}, \ldots, \gamma_{pN}]^T$, $\boldsymbol{\alpha}_p = [\alpha_{p1}, \alpha_{p2}, \ldots, \alpha_{pN}]^T$, $\mathbf{A}_p = \mathrm{diag}[\mathbf{A}_{p1}, \mathbf{A}_{p2}, \ldots, \mathbf{A}_{pN}]$, and $\mathbf{B}_p = \mathrm{diag}[\mathbf{B}_{p1}, \mathbf{B}_{p2}, \ldots, \mathbf{B}_{pN}]$ represent the parameter vectors and matrices generated by the pth IO for all receivers. $\mathbf{A}(\tau_{pq}^d)$ and $\mathbf{B}(\tau_{pq}^t, f_{pq})$ are here after referred to as $\mathbf{A}_{pq}$ and $\mathbf{B}_{pq}$, respectively. $\otimes$ is the Kronecker product operator. $\mathbf{U}_v$ is a diagonal matrix whose diagonal entries are composed of the covariance matrices of the N receiver channel noise, i.e.,

$$\mathbf{U}_v = \begin{bmatrix} \mathbf{U}_{n_1} & & \\ & \ddots & \\ & & \mathbf{U}_{n_N} \end{bmatrix}. \tag{11}$$

We define the unknown parameter vector as $\boldsymbol{\Theta} = [\boldsymbol{\gamma}^T, \boldsymbol{\alpha}^T, \boldsymbol{\tau}^T, \mathbf{f}^T]^T_{L=(6MN)\times 1}$ comprised of direct-path channel coefficients $\boldsymbol{\gamma} = [\boldsymbol{\gamma}_{11}^R, \ldots, \boldsymbol{\gamma}_{MN}^R, \boldsymbol{\gamma}_{11}^I, \ldots, \boldsymbol{\gamma}_{MN}^I]^T_{(2MN)\times 1}$, target-path channel coefficients $\boldsymbol{\alpha} = [\alpha_{11}^R, \ldots, \alpha_{MN}^R, \alpha_{11}^I, \ldots, \alpha_{MN}^I]^T_{(2MN)\times 1}$, time delay $\boldsymbol{\tau} = [\tau_{11}^t, \tau_{12}^t, \ldots, \tau_{MN}^t]^T_{(MN)\times 1}$, and Doppler frequency $\mathbf{f} = [f_{11}, f_{12}, \ldots, f_{MN}]^T_{(MN)\times 1}$ of the target. Since channel coefficients are complex, R and I represent the real and imaginary parts of the parameter, respectively. In line with [24], the elements of the FIM of $\boldsymbol{\Theta}$ are

$$[\mathbf{I}(\boldsymbol{\Theta})]_{m,n} = \mathrm{trace}\left[\mathbf{U}_y^{-1}\frac{\partial\mathbf{U}_y}{\partial\Theta_m}\mathbf{U}_y^{-1}\frac{\partial\mathbf{U}_y}{\partial\Theta_n}\right](m, n = 1, 2, \ldots, L), \tag{12}$$

where $\frac{\partial\mathbf{U}_y}{\partial\Theta_m}$ denotes the derivative of observation covariance matrix with respect to the mth element of the unknown parameter vector, whose concrete expressions are given as follows.

$$\begin{aligned}\frac{\partial\mathbf{U}_y}{\partial\boldsymbol{\gamma}_{pq}^R} = &\mathbf{A}_p[(\mathbf{E}_q\boldsymbol{\gamma}_p^H + \boldsymbol{\gamma}_p\mathbf{E}_q^H)\otimes\mathbf{U}_{x_p}]\mathbf{A}_p^H \\ &+\mathbf{B}_p[(\boldsymbol{\alpha}_p\mathbf{E}_q^H)\otimes\mathbf{U}_{x_p}]\mathbf{A}_p^H + \mathbf{A}_p[(\mathbf{E}_q\boldsymbol{\alpha}_p^H)\otimes\mathbf{U}_{x_p}]\mathbf{B}_p^H,\end{aligned} \tag{13}$$

$$\begin{aligned}\frac{\partial\mathbf{U}_y}{\partial\boldsymbol{\gamma}_{pq}^I} = &\mathbf{A}_p[(\mathbf{C}_q\boldsymbol{\gamma}_p^H + \boldsymbol{\gamma}_p\mathbf{C}_q^H)\otimes\mathbf{U}_{x_p}]\mathbf{A}_p^H \\ &+\mathbf{B}_p[(\boldsymbol{\alpha}_p\mathbf{C}_q^H)\otimes\mathbf{U}_{x_p}]\mathbf{A}_p^H + \mathbf{A}_p[(\mathbf{C}_q\boldsymbol{\alpha}_p^H)\otimes\mathbf{U}_{x_p}]\mathbf{B}_p^H,\end{aligned} \tag{14}$$

$$\frac{\partial \mathbf{U}_y}{\partial \boldsymbol{\alpha}_{pq}^R} = \mathbf{B}_p[(\mathbf{E}_q\boldsymbol{\alpha}_p^H + \boldsymbol{\alpha}_p\mathbf{E}_q^H) \otimes \mathbf{U}_{x_p}]\mathbf{B}_p^H + \mathbf{B}_p[(\mathbf{E}_q\boldsymbol{\gamma}_p^H) \otimes \mathbf{U}_{x_p}]\mathbf{A}_p^H + \mathbf{A}_p[(\boldsymbol{\gamma}_p\mathbf{E}_q^H) \otimes \mathbf{U}_{x_p}]\mathbf{B}_p^H \tag{15}$$

$$\frac{\partial \mathbf{U}_y}{\partial \boldsymbol{\alpha}_{pq}^I} = \mathbf{B}_p[(\mathbf{C}_q\boldsymbol{\alpha}_p^H + \boldsymbol{\alpha}_p\mathbf{C}_q^H) \otimes \mathbf{U}_{x_p}]\mathbf{B}_p^H + \mathbf{B}_p[(\mathbf{C}_q\boldsymbol{\gamma}_p^H) \otimes \mathbf{U}_{x_p}]\mathbf{A}_p^H + \mathbf{A}_p[(\boldsymbol{\gamma}_p\mathbf{C}_q^H) \otimes \mathbf{U}_{x_p}]\mathbf{B}_p^H, \tag{16}$$

$$\frac{\partial \mathbf{U}_y}{\partial \tau_{pq}^t} = \boldsymbol{\Gamma}_{pq}[(\boldsymbol{\alpha}_p\boldsymbol{\alpha}_p^H) \otimes \mathbf{U}_{x_p}]\mathbf{B}_p^H + \mathbf{B}_p[(\boldsymbol{\alpha}_p\boldsymbol{\alpha}_p^H) \otimes \mathbf{U}_{x_p}]\boldsymbol{\Gamma}_{pq}^H + \boldsymbol{\Gamma}_{pq}[(\boldsymbol{\alpha}_p\boldsymbol{\gamma}_p^H) \otimes \mathbf{U}_{x_p}]\mathbf{A}_p^H + \mathbf{A}_p[(\boldsymbol{\gamma}_p\boldsymbol{\alpha}_p^H) \otimes \mathbf{U}_{x_p}]\boldsymbol{\Gamma}_{pq}^H, \tag{17}$$

$$\frac{\partial \mathbf{U}_y}{\partial f_{pq}} = \boldsymbol{\Psi}_{pq}[(\boldsymbol{\alpha}_p\boldsymbol{\alpha}_p^H) \otimes \mathbf{U}_{x_p}]\mathbf{B}_p^H + \mathbf{B}_p[(\boldsymbol{\alpha}_p\boldsymbol{\alpha}_p^H) \otimes \mathbf{U}_{x_p}]\boldsymbol{\Psi}_{pq}^H + \boldsymbol{\Psi}_{pq}[(\boldsymbol{\alpha}_p\boldsymbol{\gamma}_p^H) \otimes \mathbf{U}_{x_p}]\mathbf{A}_p^H + \mathbf{A}_p[(\boldsymbol{\gamma}_p\boldsymbol{\alpha}_p^H) \otimes \mathbf{U}_{x_p}]\boldsymbol{\Psi}_{pq}^H, \tag{18}$$

where $\mathbf{E}_q$ is a column vector with N element length, whose qth element is 1 and the rest is 0, i.e., $\mathbf{E}_q = [0 \cdots 1 \cdots 0]^T$. In a similar way, $\mathbf{C}_q = [0 \cdots j \cdots 0]$, where j is the operator of the imaginary part, i.e., $j^2 = -1$. $\boldsymbol{\Gamma}_{pq}$ represents the delay-Doppler operator matrix $\mathbf{B}_p$ taking the derivative of τ_{pq}^t, which is expressed as

$$\boldsymbol{\Gamma}_{pq} = \begin{bmatrix} 0 & & & \\ & \ddots & & \\ & & \boldsymbol{\Lambda}_{pq} & \\ & & & \ddots \\ & & & & 0 \end{bmatrix}, \tag{19}$$

where

$$\boldsymbol{\Lambda}_{pq} = \boldsymbol{\varphi}(f_{pq})\mathbf{F}^H \frac{\partial \boldsymbol{\Omega}(\tau_{pq}^t)}{\partial \tau_{pq}^t}\mathbf{F}, \tag{20}$$

and

$$[\frac{\partial \boldsymbol{\Omega}(\tau_{pq}^t)}{\partial \tau_{pq}^t}]_{m,m} = \frac{-j2\pi(m-1)}{T_S N_s} e^{-j2\pi(m-1)\tau_{pq}^t/T_S N_s}, \tag{21}$$

Similarly, $\boldsymbol{\Psi}_{pq}$ is defined as

$$\boldsymbol{\Psi}_{pq} = \begin{bmatrix} 0 & & & \\ & \ddots & & \\ & & \boldsymbol{\varsigma}_{pq} & \\ & & & \ddots \\ & & & & 0 \end{bmatrix}, \tag{22}$$

where

$$\boldsymbol{\varsigma}_{pq} = \frac{\partial \boldsymbol{\varphi}(f_{pq})}{\partial f_{pq}}\mathbf{F}^H \boldsymbol{\Omega}\left(\tau_{pq}^t\right)\mathbf{F}, \tag{23}$$

and

$$[\frac{\partial \boldsymbol{\varphi}(f_{pq})}{\partial f_{pq}}]_{m,m} = j2\pi(m-1)T_s e^{j2\pi(m-1)f_{pq}T_s}. \tag{24}$$

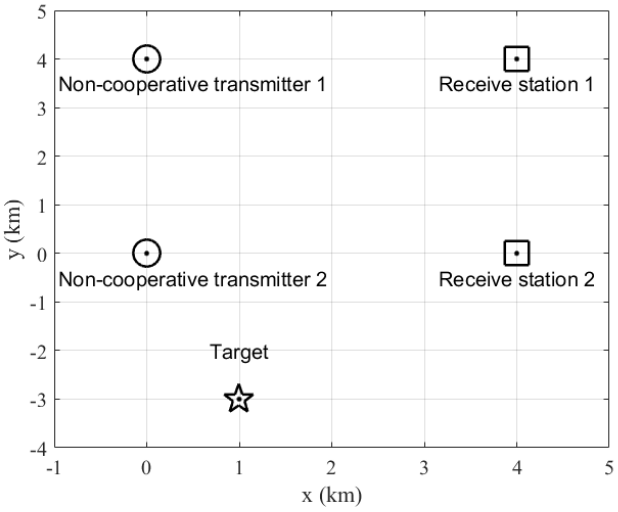

FIGURE 2. The system configuration with two IOs, two receivers, and one target.

Now, the target parameter vector of interest is defined as $\boldsymbol{\Phi} = [\boldsymbol{\gamma}^T, \alpha^T, x, y, v_x, v_y]^T_{L_p=(4MN+4)\times 1}$. According to the chain rule, we can obtain

$$\mathbf{I}(\boldsymbol{\Phi})_{L_p \times L_p} = (\frac{\partial \boldsymbol{\Theta}^T}{\partial \boldsymbol{\Phi}})\mathbf{I}(\boldsymbol{\Theta})(\frac{\partial \boldsymbol{\Theta}^T}{\partial \boldsymbol{\Phi}})^T. \tag{25}$$

$\frac{\partial \boldsymbol{\Theta}^T}{\partial \boldsymbol{\Phi}}$, the Jacobian matrix whose entries are comprised of the derivatives of formulas (3) and (4) with respect to the target position and velocity, is computed as

$$\lambda_p \frac{\partial f_{pq}}{\partial x} = -\frac{v_x}{\|\mathbf{T}_p - \mathbf{X}_t\|_2} - \frac{v_x}{\|\mathbf{R}_q - \mathbf{X}_t\|_2} - \frac{(\mathbf{T}_p - \mathbf{X}_t)^T\mathbf{X}_v(x - T_p^x)}{\|\mathbf{T}_p - \mathbf{X}_t\|_2^3} - \frac{(\mathbf{R}_q - \mathbf{X}_t)^T\mathbf{X}_v(x - R_q^x)}{\|\mathbf{R}_q - \mathbf{X}_t\|_2^3}, \tag{26}$$

$$\lambda_p \frac{\partial f_{pq}}{\partial y} = -\frac{v_y}{\|\mathbf{T}_p - \mathbf{X}_t\|_2} - \frac{v_y}{\|\mathbf{R}_q - \mathbf{X}_t\|_2} - \frac{(\mathbf{T}_p - \mathbf{X}_t)^T\mathbf{X}_v(y - T_p^y)}{\|\mathbf{T}_p - \mathbf{X}_t\|_2^3} - \frac{(\mathbf{R}_q - \mathbf{X}_t)^T\mathbf{X}_v(y - R_q^y)}{\|\mathbf{R}_q - \mathbf{X}_t\|_2^3}, \tag{27}$$

$$\lambda_p \frac{\partial f_{pq}}{\partial v_x} = \frac{T_p^x - x}{\|\mathbf{T}_p - \mathbf{X}_t\|_2} + \frac{R_q^x - x}{\|\mathbf{R}_q - \mathbf{X}_t\|_2}, \tag{28}$$

$$\lambda_p \frac{\partial f_{pq}}{\partial v_y} = \frac{T_p^y - y}{\|\mathbf{T}_p - \mathbf{X}_t\|_2} + \frac{R_q^y - y}{\|\mathbf{R}_q - \mathbf{X}_t\|_2}, \tag{29}$$

$$\frac{\partial \tau_{pq}^t}{\partial x} = \frac{1}{c}\left[\frac{x - T_p^x}{\|\mathbf{T}_p - \mathbf{X}_t\|_2} + \frac{x - R_q^x}{\|\mathbf{R}_q - \mathbf{X}_t\|_2}\right], \tag{30}$$

$$\frac{\partial \tau_{pq}^t}{\partial y} = \frac{1}{c}\left[\frac{y - T_p^y}{\|\mathbf{T}_p - \mathbf{X}_t\|_2} + \frac{y - R_q^y}{\|\mathbf{R}_q - \mathbf{X}_t\|_2}\right]. \tag{31}$$

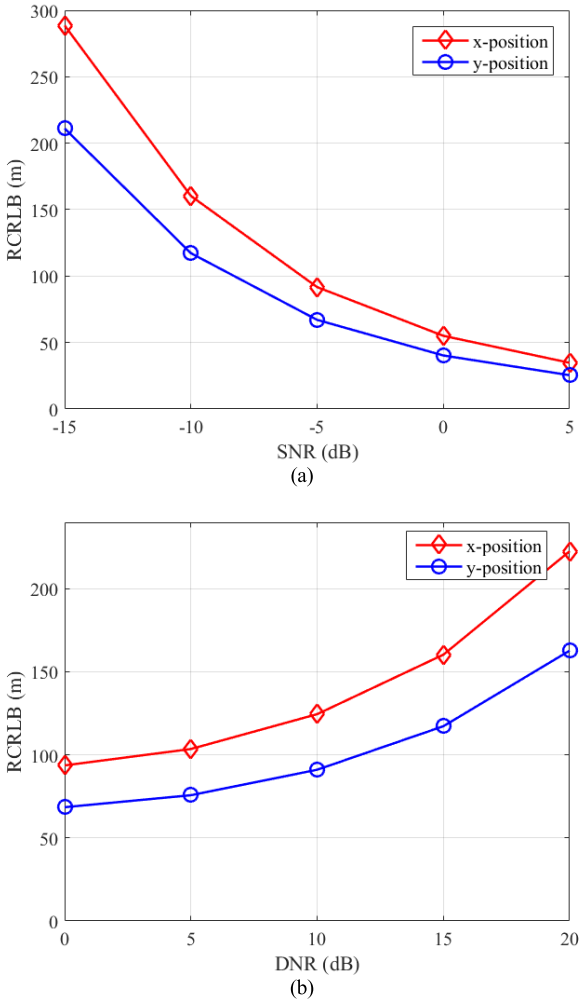

FIGURE 3. CRLB in target location dimension versus SNR and DNR. (a) Location CRLB versus SNR. (b) Location CRLB versus DNR.

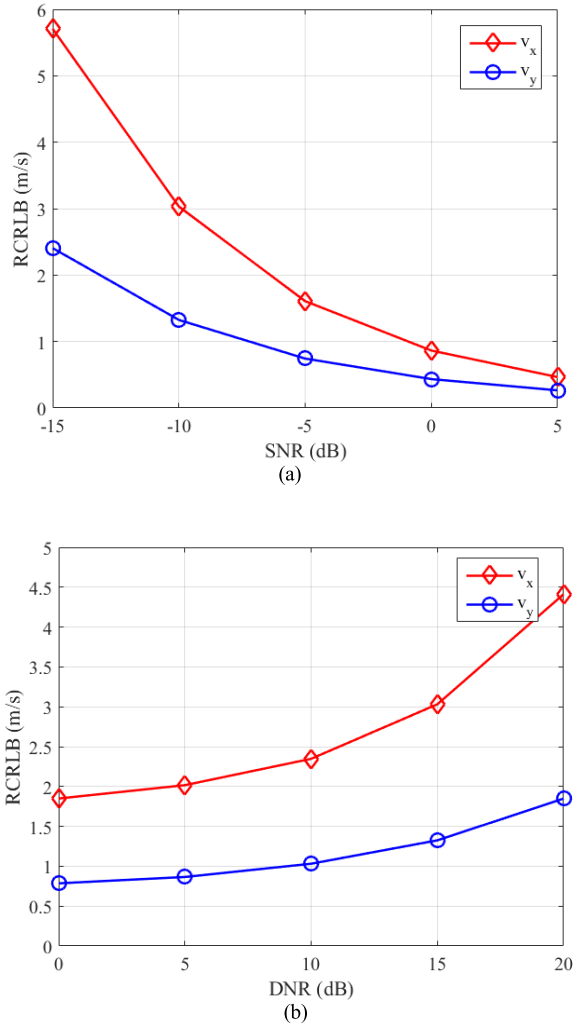

FIGURE 4. CRLB in target velocity dimension versus SNR and DNR. (a) Velocity CRLB versus SNR; (b) Velocity CRLB versus DNR.

Hence, $\frac{\partial \mathbf{\Theta}^T}{\partial \mathbf{\Phi}}$ can be rewritten as

$$\frac{\partial \mathbf{\Theta}^T}{\partial \mathbf{\Phi}} = \begin{bmatrix} \mathbf{I}_{(4MN)\times(4MN)} & \mathbf{0} \\ \mathbf{0} & \mathbf{Z}^{(f,\tau)}_{4\times(2MN)} \end{bmatrix}, \tag{32}$$

where $\mathbf{I}_{(4MN)\times(4MN)}$ is the unit matrix, and

$$\mathbf{Z}^{(f,\tau)} = \begin{bmatrix} \frac{\partial \tau^t_{11}}{\partial x} & \cdots & \frac{\partial \tau^t_{MN}}{\partial x} & \frac{\partial f_{11}}{\partial x} & \cdots & \frac{\partial f_{MN}}{\partial x} \\ \frac{\partial \tau^t_{11}}{\partial y} & \cdots & \frac{\partial \tau^t_{MN}}{\partial y} & \frac{\partial f_{11}}{\partial y} & \cdots & \frac{\partial f_{MN}}{\partial y} \\ 0 & \cdots & 0 & \frac{\partial f_{11}}{\partial v_x} & \cdots & \frac{\partial f_{MN}}{\partial v_x} \\ 0 & \cdots & 0 & \frac{\partial f_{11}}{\partial v_y} & \cdots & \frac{\partial f_{MN}}{\partial v_y} \end{bmatrix}. \tag{33}$$

Therefore, the CRLB of interest in this paper is

$$\mathrm{CRLB}(\mathbf{\Phi}) = \mathbf{I}^{-1}(\mathbf{\Phi}), \tag{34}$$

where the CRLB for each parameter is given as

$$\mathrm{CRLB}_{\Phi_m} = \left[\mathbf{I}^{-1}(\mathbf{\Phi})\right]_{m,m} (m = 1, 2, ..., L_P). \tag{35}$$

IV. SIMULATION RESULTS

Numerical simulation results will be taken over in this section to compute the CRLB for a stochastic process based multistatic passive radar network with DPI. Parts of the simulation parameters in [19] are used for reference, and a multistatic configuration with two IOs and two receivers (See Fig. 2) is considered. The location states of IOs and receivers are set as

$$\mathbf{T}_1 = [0, 0]^T \text{ km}, \quad \mathbf{T}_2 = [0, 4]^T \text{ km},$$
$$\mathbf{R}_1 = [4, 0]^T \text{ km}, \quad \mathbf{R}_2 = [4, 4]^T \text{ km}.$$

For simplicity, only one target located at $[1, -3]^T$km with velocity states $[30, 50]^T$ m/s is considered in this scenario. In simulation, first-order AR process is employed to model the signals transmitted by IOs. We set the waveform parameters be the same as in [24]. Since we emphasize on the impact of parameter changes on the CRLB, the same parameters of different IOs are assumed to remain the same, e.g., $\lambda_1 = \lambda_2 = \cdots = \lambda_M = \lambda$, $N_{c_1} = N_{c_2} = \cdots N_{c_M} = N_c$, and $\rho_1 = \rho_2 = \cdots \rho_M = \rho$. Let $N_s = 256$, $N_c = 200$, $\rho = -0.9$,

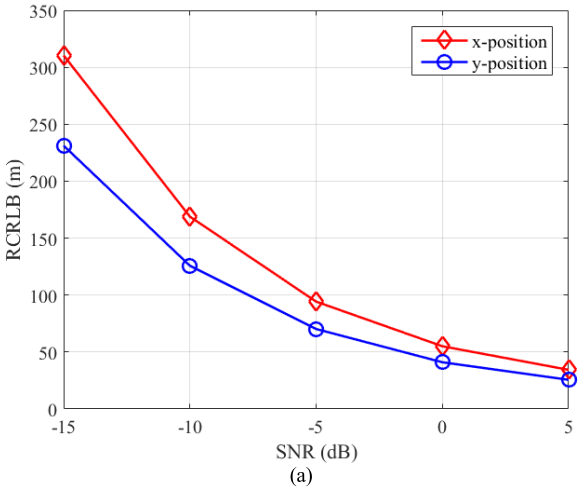

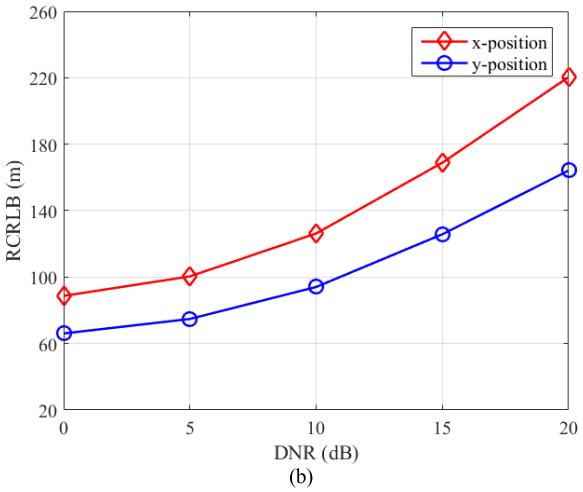

FIGURE 5. CRLB in target location dimension versus SNR and DNR after changing the geometry. (a) Location CRLB versus SNR; (b) Location CRLB versus DNR.

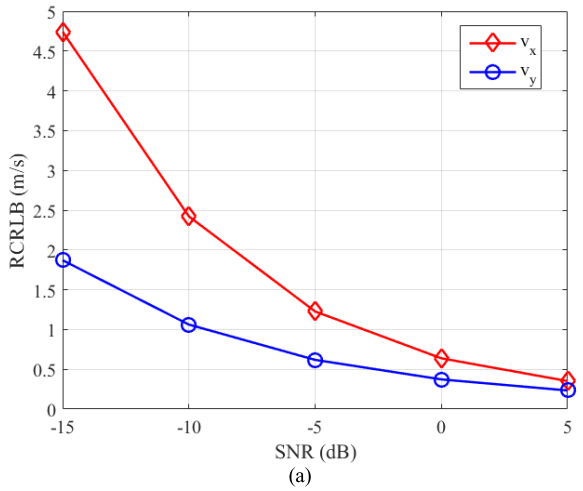

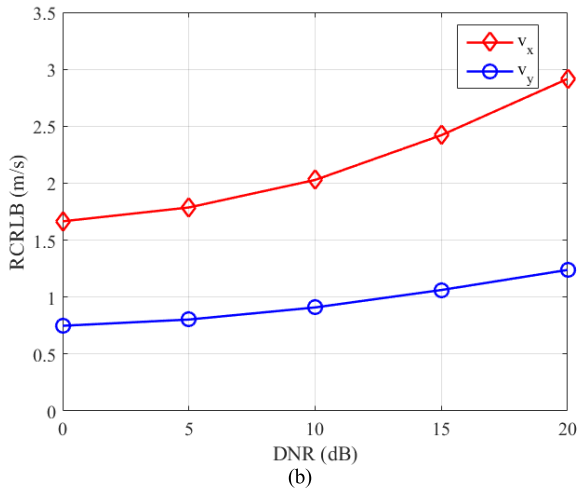

FIGURE 6. CRLB in target velocity dimension versus SNR and DNR after changing the geometry. (a) Velocity CRLB versus SNR. (b) Velocity CRLB versus DNR.

$T_s = 1$, and $\lambda = 3$m. In terms of the configuration shown in Fig. 1, the SNR and DNR are defined as

$$\text{SNR} = 10\log_{10}\sum_{p=1}^{M}\sum_{q=1}^{N}\frac{|\alpha_{pq}|^2}{\sigma_q^2}, \tag{36}$$

$$\text{DNR} = 10\log_{10}\sum_{p=1}^{M}\sum_{q=1}^{N}\frac{|\gamma_{pq}|^2}{\sigma_q^2}. \tag{37}$$

It is supposed to note that the SNR and DNR of each receiver remain the same, and fix $\sigma_1^2 = \sigma_2^2 \cdots = \sigma_N^2 = 1$. The square root of CRLB (RCRLB) will be computed in each analysis.

Fig. 3 illustrates how the CRLB in target location dimension changes as SNR and DNR increase. We set DNR $=$ 15dB and SNR $= -10$dB in Figs. 3 (a) and (b), respectively. In Fig. 4, the results of the velocity CRLB against SNR and DNR are rendered, where the SNR and DNR are the same as defined in Fig. 3. Relying on obtained results, one can find that the SNR and DNR noticeably affect the CRLB. Specifically, both the location CRLB and the velocity CRLB decrease with increasing SNR, and increase with increasing DNR. Moreover, the CRLB in the y-axis component is lower than the x-axis component for both location and velocity, which means the estimation of the unknown target parameters in the y-dimension might obtain better performance. Furthermore, the curves as a function of SNR in Figs. 3 and 4 decrease more and more slowly as the SNR becomes stronger. However, the increasing DNR exacerbate the estimation performance more and more significant.

Next, the effect of the geographical distribution of the passive radar network on the target location and velocity CRLB is analyzed through an illustrative example. Since the position of the IO is generally fixed in practice, this analysis is achieved by only adjusting the locations of the receivers. Let the positions of receive station 1 and receive station 2 be changed to $[5, 4]^T$ km and $[5, 0]^T$ km, respectively. The CRLB calculation results are plotted in Fig. 5 and Fig. 6. As one can see that changing the geometry will affect the variation of the CRLB. The trend of the curves with varying SNR and DNR is analogous to that depicted in the first configuration.

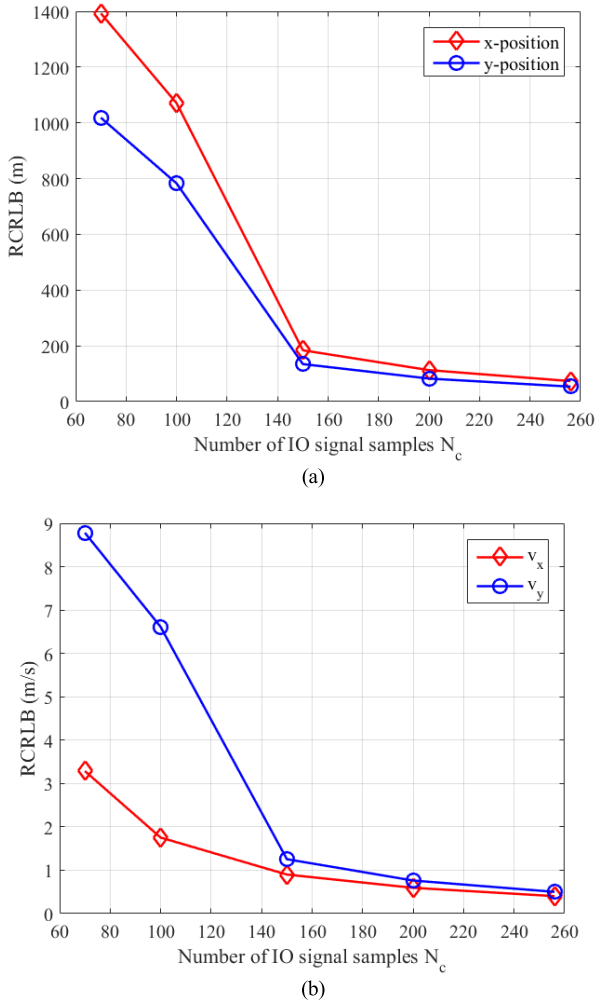

FIGURE 7. The location and velocity CRLB versus the number of IO signal samples. (a) CRLB in location dimension. (b) CRLB in velocity dimension.

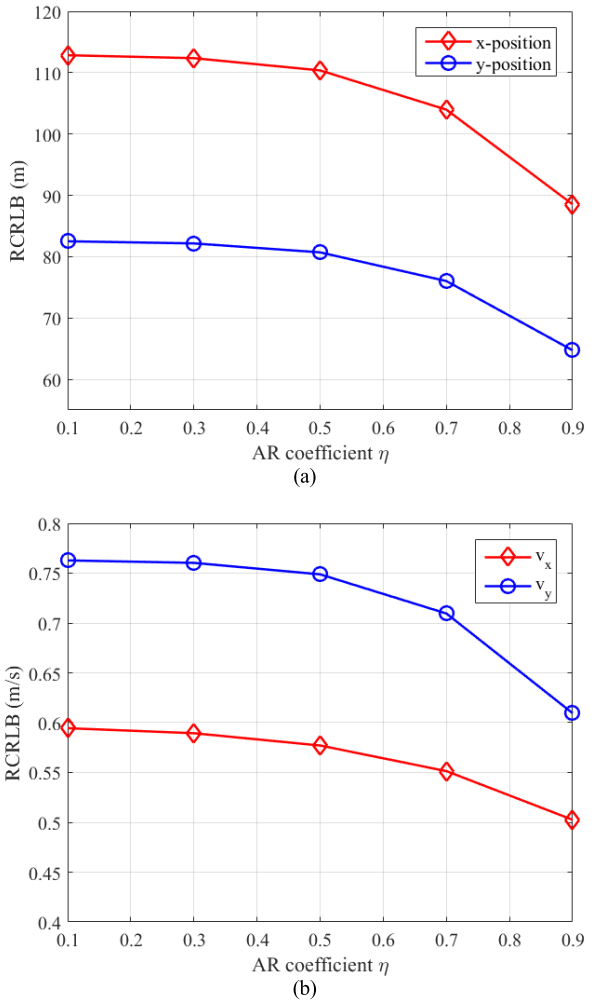

FIGURE 8. The location and velocity CRLB versus AR coefficient. (a) CRLB in location dimension. (b) CRLB in velocity dimension.

Besides, the CRLB in the y-dimension is still lower than that in the x-dimension. Differently, the second configuration after changing the geometry has a certain performance regression of CRLB on location, whereas a little improvement on velocity.

In what follows, the system geometry remains unchanged as presented in Fig. 2, i.e., the first configuration. The curves of CRLB as a function of signal parameters are displayed in Fig. 7 and Fig. 8, where the SNR and DNR are both set as 0dB and -10dB. In Fig. 7, the results depict how the CRLB changes with regard to varying number of the IO signal samples N_c, which indirectly reflects the relationship with the signal duration T. Intuitively, as the N_c is increased, there is a decrease in the CRLB for the parameters. This is reasonable because more IO signal samples represent longer signal duration, which illustrates that more useful information will be included in the received measurement, that is, the system is able to obtain more dramatical improvement of the estimation performance.

Fig. 8 gives detailed insights into the CRLB performance on location and velocity dimensions according to varying IO waveform correlations. Note that η represents the absolute value of the AR coefficient, i.e., $\eta = |\rho|$. One obvious feature is that the CRLB performance is gradually facilitated as η increases. Moreover, the sensitivity of both location and velocity CRLB to the correlation between the IO waveform samples will become stronger as η increases. This is expected since larger η denotes stronger correlation between the IO waveform samples under the adopted signal model in this work. When the IO waveform is highly correlated, there will exist extensive potential waveform information that can be utilized for enhancing the estimation performance.

We also investigate the impacts of multipath clutter on CRLB. According to (1), the received signal model after considering multipath components is rewritten as

$$y_q(t) = \sum_{p=1}^{M} \gamma_{pq} x_p(t - \tau_{pq}^d) + \sum_{p=1}^{M} \alpha_{pq} x_p(t - \tau_{pq}^t) e^{j2\pi f_{pq} t} + \sum_{p=1}^{M} \sum_{w=1}^{W_{pq}^c} \delta_{pq}^w x_p(t - \tau_{pq}^w) + n_q(t), \quad (38)$$

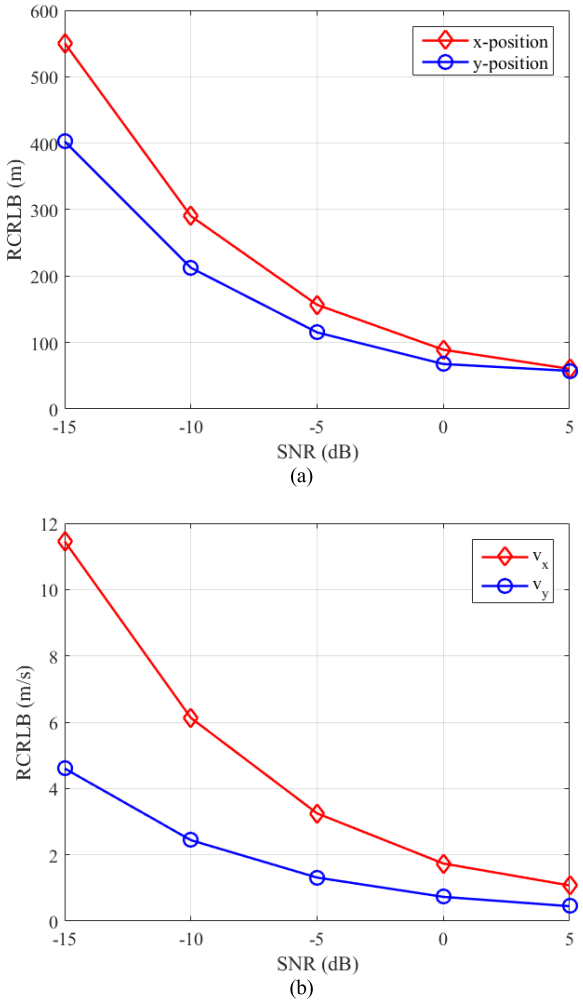

FIGURE 9. The location and velocity CRLB versus SNR while considering multipath components. (a) CRLB in location dimension. (b) CRLB in velocity dimension.

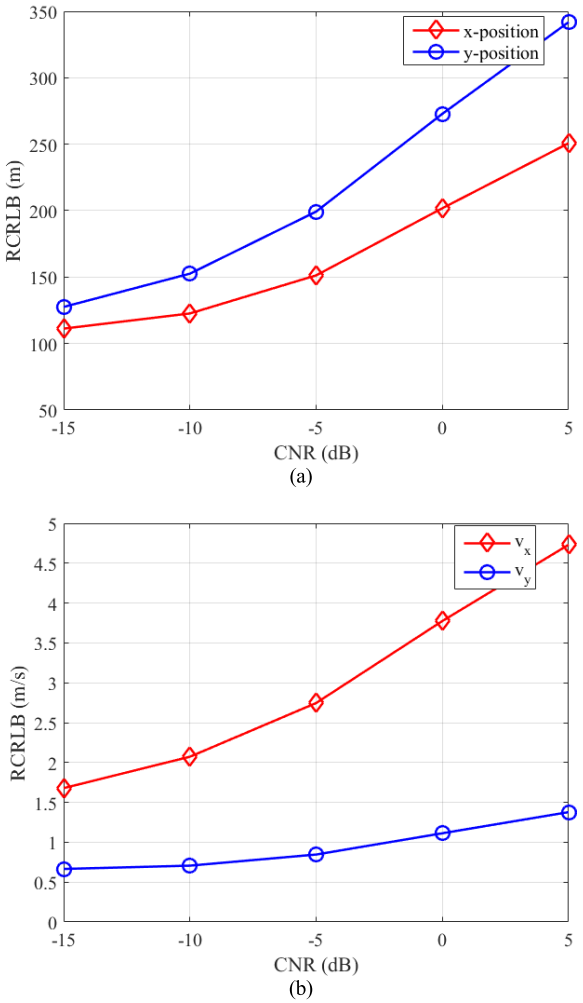

FIGURE 10. The location and velocity CRLB versus CNR. (a) CRLB in location dimension. (b) CRLB in velocity dimension.

where W_{pq}^{c} is the number of clutter components of the pqth bistatic pair, and δ_{pq}^{w} and τ_{pq}^{w} denote the associated complex channel coefficient and time delay of the wth multipath component, respectively. For simplicity, we assume that only one multipath clutter exists in each pqth transmitter-receiver path. Hence, the received signal model is simplified as

$$y_q(t) = \sum_{p=1}^{M} \gamma_{pq} x_p(t - \tau_{pq}^{d}) + \sum_{p=1}^{M} \alpha_{pq} x_p(t - \tau_{pq}^{t}) e^{j2\pi f_{pq} t} + \sum_{p=1}^{M} \delta_{pq} x_p(t - \tau_{pq}^{c}) + n_q(t). \quad (39)$$

The specific derivation of CRLB in this case is demonstrated in Appendix A. Herein, the CNR is defined as

$$\mathrm{CNR} = 10 \log_{10} \sum_{p=1}^{M} \sum_{q=1}^{N} \frac{|\delta_{pq}|^2}{\sigma_q^2}. \quad (40)$$

The curve of CRLB with varying SNR is taken as an example to study how multipath clutter affects the estimation performance, where CNR = 20dB and other parameters keep the same as defined in Fig. 2. The results are plotted in Fig. 9 with multipath delay assigned as $1.05\tau_{11}^{d}$, $1.15\tau_{12}^{d}$, $1.25\tau_{21}^{d}$, and $1.35\tau_{22}^{d}$. One can observe that there exists a significant performance degradation on CRLB when the multipath components of the transmitted signal are considered.

In Fig. 10, we demonstrate the relationship between the CRLB and the CNR. The multipath delays remain the same as Fig. 9 with the SNR and DNR set as 5dB and -10dB, respectively. It can be seen that the CRLB curves on both position and velocity dimension shift upward more and more significant as CNR increases. Hence, in practice, multipath interference should be suppressed as much as possible.

V. CONCLUSION

In this paper, we have completed a detailed investigation of the joint estimation for target location and velocity in the passive radar system comprised of multiple noncooperative transmitters and geographically distributed receive stations based on stochastic process model. The CRLB for a single target is computed with the absence of reference channel

and the existence of DPI. We observe that the joint CRLB value is a function of both the system geometry and the IO waveform parameters. Furthermore, numerical results have been revealed to validate that the CRLB is dependent on SNR, DNR, and CNR. In future work, the computation will be extended to the case, where multiple targets are taken into account. Additionally, the problem of transmitter selection and optimal receiver arrangement strategy will be studied.

APPENDIX

A. Derivation of CRLB considering multipath components

According to (39), the digitized expression of the received signal is expressed as

$$\mathbf{y}_q = \sum_{p=1}^{M} \gamma_{pq}\mathbf{A}(\tau_{pq}^d)\mathbf{x}_p + \sum_{p=1}^{M} \alpha_{pq}\mathbf{B}(\tau_{pq}^t, f_{pq})\mathbf{x}_p + \sum_{p=1}^{M} \delta_{pq}\mathbf{W}(\tau_{pq}^c)\mathbf{x}_p + \mathbf{n}_q, \quad (41)$$

where $\mathbf{W}(\tau_{pq}^c)$ is the delay operator for multipath signal, which is denoted as

$$\mathbf{W}(\tau_{pq}^c) = \mathbf{F}^H \mathbf{\Omega}(\tau_{pq}^c)\mathbf{F}. \quad (42)$$

The covariance matrix of joint measurements $\mathbf{y}$ is

$$\begin{aligned}\mathbf{U}_y = \sum_{p=1}^{M} \{&\mathbf{A}_p[(\boldsymbol{\gamma}_p\boldsymbol{\gamma}_p^H)\otimes\mathbf{U}_{x_p}]\mathbf{A}_p^H + \mathbf{B}_p[(\boldsymbol{\alpha}_p\boldsymbol{\alpha}_p^H)\otimes\mathbf{U}_{x_p}]\mathbf{B}_p^H \\ &+ \mathbf{B}_p[(\boldsymbol{\alpha}_p\boldsymbol{\gamma}_p^H)\otimes\mathbf{U}_{x_p}]\mathbf{A}_p^H + \mathbf{A}_p[(\boldsymbol{\gamma}_p\boldsymbol{\alpha}_p^H)\otimes\mathbf{U}_{x_p}]\mathbf{B}_p^H \\ &+ \mathbf{A}_p[(\boldsymbol{\gamma}_p\boldsymbol{\delta}_p^H)\otimes\mathbf{U}_{x_p}]\mathbf{W}_p^H + \mathbf{B}_p[(\boldsymbol{\alpha}_p\boldsymbol{\delta}_p^H)\otimes\mathbf{U}_{x_p}]\mathbf{W}_p^H \\ &+ \mathbf{W}_p[(\boldsymbol{\delta}_p\boldsymbol{\delta}_p^H)\otimes\mathbf{U}_{x_p}]\mathbf{W}_p^H + \mathbf{W}_p[(\boldsymbol{\delta}_p\boldsymbol{\gamma}_p^H)\otimes\mathbf{U}_{x_p}]\mathbf{A}_p^H \\ &+ \mathbf{W}_p[(\boldsymbol{\delta}_p\boldsymbol{\alpha}_p^H)\otimes\mathbf{U}_{x_p}]\mathbf{B}_p^H\} + \mathbf{U}_v, \end{aligned} \quad (43)$$

where $\boldsymbol{\delta}_p = [\delta_{p1}, \delta_{p2}, \ldots \delta_{pN}]^T$ and $\mathbf{W}_p = \mathrm{diag}[\mathbf{W}_{p1}, \mathbf{W}_{p2}, \ldots, \mathbf{W}_{pN}]$. Here, $\mathbf{W}_{pq}$ is the simple representation of $\mathbf{W}(\tau_{pq}^c)$. Under this circumstances, the unknown parameter vector is redefined as

$$\mathbf{\Theta} = [\boldsymbol{\gamma}^T, \boldsymbol{\alpha}^T, \boldsymbol{\delta}^T, \boldsymbol{\tau}^T, \mathbf{f}^T, \boldsymbol{\tau}_c^T]^T_{L=(9MN)\times 1}, \quad (44)$$

where $\boldsymbol{\delta} = [\delta_{11}^R, \ldots, \delta_{MN}^R, \delta_{11}^I, \ldots, \delta_{MN}^I]^T_{(2MN)\times 1}$ and $\boldsymbol{\tau}_c = [\tau_{11}^c, \tau_{12}^c, \ldots, \tau_{MN}^c]^T_{(MN)\times 1}$. Hence, in the light of (12), the derivatives of $\mathbf{U}_y$ with respect to the unknown parameters in (43) are expressed as follows.

$$\begin{aligned}\frac{\partial \mathbf{U}_y}{\partial \boldsymbol{\gamma}_{pq}^R} = &\mathbf{A}_p[(\mathbf{E}_q\boldsymbol{\gamma}_p^H + \boldsymbol{\gamma}_p\mathbf{E}_q^H)\otimes\mathbf{U}_{x_p}]\mathbf{A}_p^H \\ &+ \mathbf{B}_p[(\boldsymbol{\alpha}_p\mathbf{E}_q^H)\otimes\mathbf{U}_{x_p}]\mathbf{A}_p^H + \mathbf{A}_p[(\mathbf{E}_q\boldsymbol{\alpha}_p^H)\otimes\mathbf{U}_{x_p}]\mathbf{B}_p^H \\ &+ \mathbf{A}_p[(\mathbf{E}_q\boldsymbol{\delta}_p^H)\otimes\mathbf{U}_{x_p}]\mathbf{W}_p^H + \mathbf{W}_p[(\boldsymbol{\delta}_p\mathbf{E}_q^H)\otimes\mathbf{U}_{x_p}]\mathbf{A}_p^H, \end{aligned} \quad (45)$$

$$\begin{aligned}\frac{\partial \mathbf{U}_y}{\partial \boldsymbol{\gamma}_{pq}^I} = &\mathbf{A}_p[(\mathbf{C}_q\boldsymbol{\gamma}_p^H + \boldsymbol{\gamma}_p\mathbf{C}_q^H)\otimes\mathbf{U}_{x_p}]\mathbf{A}_p^H \\ &+ \mathbf{B}_p[(\boldsymbol{\alpha}_p\mathbf{C}_q^H)\otimes\mathbf{U}_{x_p}]\mathbf{A}_p^H + \mathbf{A}_p[(\mathbf{C}_q\boldsymbol{\alpha}_p^H)\otimes\mathbf{U}_{x_p}]\mathbf{B}_p^H \\ &+ \mathbf{A}_p[(\mathbf{C}_q\boldsymbol{\delta}_p^H)\otimes\mathbf{U}_{x_p}]\mathbf{W}_p^H + \mathbf{W}_p[(\boldsymbol{\delta}_p\mathbf{C}_q^H)\otimes\mathbf{U}_{x_p}]\mathbf{A}_p^H, \end{aligned} \quad (46)$$

$$\begin{aligned}\frac{\partial \mathbf{U}_y}{\partial \boldsymbol{\alpha}_{pq}^R} = &\mathbf{B}_p[(\mathbf{E}_q\boldsymbol{\alpha}_p^H + \boldsymbol{\alpha}_p\mathbf{E}_q^H)\otimes\mathbf{U}_{x_p}]\mathbf{B}_p^H \\ &+ \mathbf{B}_p[(\mathbf{E}_q\boldsymbol{\gamma}_p^H)\otimes\mathbf{U}_{x_p}]\mathbf{A}_p^H + \mathbf{A}_p[(\boldsymbol{\gamma}_p\mathbf{E}_q^H)\otimes\mathbf{U}_{x_p}]\mathbf{B}_p^H \\ &+ \mathbf{B}_p[(\mathbf{E}_q\boldsymbol{\delta}_p^H)\otimes\mathbf{U}_{x_p}]\mathbf{W}_p^H + \mathbf{W}_p[(\boldsymbol{\delta}_p\mathbf{E}_q^H)\otimes\mathbf{U}_{x_p}]\mathbf{B}_p^H, \end{aligned} \quad (47)$$

$$\begin{aligned}\frac{\partial \mathbf{U}_y}{\partial \boldsymbol{\alpha}_{pq}^I} = &\mathbf{B}_p[(\mathbf{C}_q\boldsymbol{\alpha}_p^H + \boldsymbol{\alpha}_p\mathbf{C}_q^H)\otimes\mathbf{U}_{x_p}]\mathbf{B}_p^H \\ &+ \mathbf{B}_p[(\mathbf{C}_q\boldsymbol{\gamma}_p^H)\otimes\mathbf{U}_{x_p}]\mathbf{A}_p^H + \mathbf{A}_p[(\boldsymbol{\gamma}_p\mathbf{C}_q^H)\otimes\mathbf{U}_{x_p}]\mathbf{B}_p^H \\ &+ \mathbf{B}_p[(\mathbf{C}_q\boldsymbol{\delta}_p^H)\otimes\mathbf{U}_{x_p}]\mathbf{W}_p^H + \mathbf{W}_p[(\boldsymbol{\delta}_p\mathbf{C}_q^H)\otimes\mathbf{U}_{x_p}]\mathbf{B}_p^H, \end{aligned} \quad (48)$$

$$\begin{aligned}\frac{\partial \mathbf{U}_y}{\partial \boldsymbol{\delta}_{pq}^R} = &\mathbf{W}_p[(\mathbf{E}_q\boldsymbol{\delta}_p^H + \boldsymbol{\delta}_p\mathbf{E}_q^H)\otimes\mathbf{U}_{x_p}]\mathbf{W}_p^H \\ &+ \mathbf{B}_p[(\boldsymbol{\alpha}_p\mathbf{E}_q^H)\otimes\mathbf{U}_{x_p}]\mathbf{W}_p^H + \mathbf{A}_p[(\boldsymbol{\gamma}_p\mathbf{E}_q^H)\otimes\mathbf{U}_{x_p}]\mathbf{W}_p^H \\ &+ \mathbf{W}_p[(\mathbf{E}_q\boldsymbol{\gamma}_p^H)\otimes\mathbf{U}_{x_p}]\mathbf{A}_p^H + \mathbf{W}_p[(\mathbf{E}_q\boldsymbol{\alpha}_p^H)\otimes\mathbf{U}_{x_p}]\mathbf{B}_p^H, \end{aligned} \quad (49)$$

$$\begin{aligned}\frac{\partial \mathbf{U}_y}{\partial \boldsymbol{\delta}_{pq}^I} = &\mathbf{W}_p[(\mathbf{C}_q\boldsymbol{\delta}_p^H + \boldsymbol{\delta}_p\mathbf{C}_q^H)\otimes\mathbf{U}_{x_p}]\mathbf{W}_p^H \\ &+ \mathbf{B}_p[(\boldsymbol{\alpha}_p\mathbf{C}_q^H)\otimes\mathbf{U}_{x_p}]\mathbf{W}_p^H + \mathbf{A}_p[(\boldsymbol{\gamma}_p\mathbf{C}_q^H)\otimes\mathbf{U}_{x_p}]\mathbf{W}_p^H \\ &+ \mathbf{W}_p[(\mathbf{C}_q\boldsymbol{\gamma}_p^H)\otimes\mathbf{U}_{x_p}]\mathbf{A}_p^H + \mathbf{W}_p[(\mathbf{C}_q\boldsymbol{\alpha}_p^H)\otimes\mathbf{U}_{x_p}]\mathbf{B}_p^H, \end{aligned} \quad (50)$$

$$\begin{aligned}\frac{\partial \mathbf{U}_y}{\partial \tau_{pq}^t} = &\mathbf{\Gamma}_{pq}[(\boldsymbol{\alpha}_p\boldsymbol{\alpha}_p^H)\otimes\mathbf{U}_{x_p}]\mathbf{B}_p^H + \mathbf{B}_p[(\boldsymbol{\alpha}_p\boldsymbol{\alpha}_p^H)\otimes\mathbf{U}_{x_p}]\mathbf{\Gamma}_{pq}^H \\ &+ \mathbf{\Gamma}_{pq}[(\boldsymbol{\alpha}_p\boldsymbol{\gamma}_p^H)\otimes\mathbf{U}_{x_p}]\mathbf{A}_p^H + \mathbf{A}_p[(\boldsymbol{\gamma}_p\boldsymbol{\alpha}_p^H)\otimes\mathbf{U}_{x_p}]\mathbf{\Gamma}_{pq}^H \\ &+ \mathbf{\Gamma}_{pq}[(\boldsymbol{\alpha}_p\boldsymbol{\delta}_p^H)\otimes\mathbf{U}_{x_p}]\mathbf{W}_p^H + \mathbf{W}_p[(\boldsymbol{\gamma}_p\boldsymbol{\delta}_p^H)\otimes\mathbf{U}_{x_p}]\mathbf{\Gamma}_{pq}^H, \end{aligned} \quad (51)$$

$$\begin{aligned}\frac{\partial \mathbf{U}_y}{\partial f_{pq}} = &\mathbf{\Psi}_{pq}[(\boldsymbol{\alpha}_p\boldsymbol{\alpha}_p^H)\otimes\mathbf{U}_{x_p}]\mathbf{B}_p^H + \mathbf{B}_p[(\boldsymbol{\alpha}_p\boldsymbol{\alpha}_p^H)\otimes\mathbf{U}_{x_p}]\mathbf{\Psi}_{pq}^H \\ &+ \mathbf{\Psi}_{pq}[(\boldsymbol{\alpha}_p\boldsymbol{\gamma}_p^H)\otimes\mathbf{U}_{x_p}]\mathbf{A}_p^H + \mathbf{A}_p[(\boldsymbol{\gamma}_p\boldsymbol{\alpha}_p^H)\otimes\mathbf{U}_{x_p}]\mathbf{\Psi}_{pq}^H \\ &+ \mathbf{\Psi}_{pq}[(\boldsymbol{\alpha}_p\boldsymbol{\delta}_p^H)\otimes\mathbf{U}_{x_p}]\mathbf{W}_p^H + \mathbf{W}_p[(\boldsymbol{\delta}_p\boldsymbol{\alpha}_p^H)\otimes\mathbf{U}_{x_p}]\mathbf{\Psi}_{pq}^H, \end{aligned} \quad (52)$$

$$\begin{aligned}\frac{\partial \mathbf{U}_y}{\partial \tau_{pq}^c} = &\mathbf{A}_p[(\boldsymbol{\gamma}_p\boldsymbol{\delta}_p^H)\otimes\mathbf{U}_{x_p}]\boldsymbol{\xi}_{pq}^H + \mathbf{B}_p[(\boldsymbol{\alpha}_p\boldsymbol{\delta}_p^H)\otimes\mathbf{U}_{x_p}]\boldsymbol{\xi}_{pq}^H \\ &+ \boldsymbol{\xi}_{pq}[(\boldsymbol{\delta}_p\boldsymbol{\delta}_p^H)\otimes\mathbf{U}_{x_p}]\mathbf{W}_p^H + \mathbf{W}_p[(\boldsymbol{\delta}_p\boldsymbol{\delta}_p^H)\otimes\mathbf{U}_{x_p}]\boldsymbol{\xi}_{pq}^H \\ &+ \boldsymbol{\xi}_{pq}[(\boldsymbol{\delta}_p\boldsymbol{\gamma}_p^H)\otimes\mathbf{U}_{x_p}]\mathbf{A}_p^H + \boldsymbol{\xi}_{pq}[(\boldsymbol{\delta}_p\boldsymbol{\alpha}_p^H)\otimes\mathbf{U}_{x_p}]\mathbf{B}_p^H, \end{aligned} \quad (53)$$

where ξ_{pq} is the derivative of $\mathbf{W}_p$ with respect to τ_{pq}^c, which is expressed as

$$\xi_{pq} = \begin{bmatrix} 0 & & & \\ & \ddots & & \\ & & \mathbf{\Pi}_{pq} & \\ & & & \ddots \\ & & & 0 \end{bmatrix}, \quad (54)$$

where

$$\mathbf{\Pi}_{pq} = \mathbf{F}^H \frac{\partial \mathbf{\Omega}(\tau_{pq}^c)}{\partial \tau_{pq}^c}\mathbf{F}, \quad (55)$$

and

$$\left[\frac{\partial \mathbf{\Omega}(\tau_{pq}^c)}{\partial \tau_{pq}^c}\right]_{m,m} = \frac{-j2\pi(m-1)}{T_s N_s} e^{-j2\pi(m-1)\tau_{pq}^c/T_s N_s}. \quad (56)$$

The target parameter vector $\mathbf{\Phi}$ is changed to

$$\mathbf{\Phi} = [\boldsymbol{\gamma}^T, \boldsymbol{\alpha}^T, \boldsymbol{\delta}^T, x, y, v_x, v_y]^T_{L_p'=(6MN+4)\times 1}. \quad (57)$$

The FIM of $\mathbf{\Phi}$ is calculated using (25), and $\frac{\partial \mathbf{\Theta}^T}{\partial \mathbf{\Phi}}$ has a similar representation to (32), i.e.,

$$\frac{\partial \mathbf{\Theta}^T}{\partial \Phi'} = \begin{bmatrix} \mathbf{I}_{(6MN)\times(6MN)} & \mathbf{0} \\ \mathbf{0} & \mathbf{Z}'^{(f,\tau)}_{4\times(3MN)} \end{bmatrix}, \quad (58)$$

where

$$\mathbf{Z}'^{(f,\tau)} = \begin{bmatrix} \frac{\partial \tau_{11}^t}{\partial x} & \cdots & \frac{\partial \tau_{MN}^t}{\partial x} & \frac{\partial f_{11}}{\partial x} & \cdots & \frac{\partial f_{MN}}{\partial x} & 0 \cdots 0 \\ \frac{\partial \tau_{11}^t}{\partial y} & \cdots & \frac{\partial \tau_{MN}^t}{\partial y} & \frac{\partial f_{11}}{\partial y} & \cdots & \frac{\partial f_{MN}}{\partial y} & 0 \cdots 0 \\ 0 & \cdots & 0 & \frac{\partial f_{11}}{\partial v_x} & \cdots & \frac{\partial f_{MN}}{\partial v_x} & 0 \cdots 0 \\ 0 & \cdots & 0 & \frac{\partial f_{11}}{\partial v_y} & \cdots & \frac{\partial f_{MN}}{\partial v_y} & 0 \cdots 0 \end{bmatrix}. \quad (59)$$

Finally, the CRLB for each target parameter is calculated by (35).

REFERENCES

[1] X. Zhang, H. Li, and B. Himed, "Maximum likelihood delay and Doppler estimation for passive sensing," *IEEE Sensors J.*, vol. 19, no. 1, pp. 180–188, Jan. 2019.

[2] X. Zhang, J. Sward, H. Li, A. Jakobsson, and B. Himed, "A sparsity-based passive multistatic detector," *IEEE Trans. Aerosp. Electron. Syst.*, to be published. doi: 10.1109/TAES.2019.2895710.

[3] S. Gogineni, P. Setlur, M. Rangaswamy, and R. R. Nadakuditi, "Passive radar detection with noisy reference channel using principal subspace similarity," *IEEE Trans. Aerosp. Electron. Syst.*, vol. 54, no. 1, pp. 18–36, Feb. 2018.

[4] H. Ma, M. Antoniou, D. Pastina, F. Santi, F. Pieralice, M. Bucciarelli, and M. Cherniakov, "Maritime moving target indication using passive GNSS-based bistatic radar," *IEEE Trans. Aerosp. Electron. Syst.*, vol. 54, no. 1, pp. 115–130, Feb. 2018.

[5] J. Yi, X. Wan, D. Li, and H. Leung, "Robust clutter rejection in passive radar via generalized subband cancellation," *IEEE Trans. Aerosp. Electron. Syst.*, vol. 54, no. 4, pp. 1931–1946, Aug. 2018.

[6] S. R. Stevens and J. A. Jackson, "Emitter selection criteria for passive multistatic synthetic aperture radar imaging," *IET Radar Sonar Navigat.*, vol. 8, no. 9, pp. 1267–1279, Dec. 2014.

[7] S. A. Kaiser, A. J. Christianson, and R. M. Narayanan, "Multistatic Doppler estimation using global positioning system passive coherent location," *IEEE Trans. Aerosp. Electron. Syst.*, to be published. doi: 10.1109/TAES.2019.2899771.

[8] D. Gromek, K. Radecki, J. Drozdowicz, P. Samczynski, and J. Szabatin, "Passive SAR imaging using DVB-T illumination for airborne applications," *IET Radar, Sonar Navigat.*, vol. 13, no. 2, pp. 213–221, Feb. 2019.

[9] G. Bournaka, M. Ummenhofer, D. Cristallini, J. Palmer, and A. Summers, "Experimental study for transmitter imperfections in DVB-T based passive radar," *IEEE Trans. Aerosp. Electron. Syst.*, vol. 54, no. 3, pp. 1341–1354, Jun. 2018.

[10] G.-H. Park, D.-G. Kim, H. J. Kim, and H.-N. Kim, "Maximum-likelihood angle estimator for multi-channel FM-radio-based passive coherent location," *IET Radar, Sonar Navigat.*, vol. 12, no. 6, pp. 617–625, Jun. 2018.

[11] A. Zaimbashi, "Broadband target detection algorithm in FM-based passive bistatic radar systems," *IET Radar, Sonar Navigat.*, vol. 10, no. 8, pp. 1485–1499, 2016.

[12] F. Colone, T. Martelli, and P. Lombardo, "Quasi-monostatic versus near forward scatter geometry in WiFi-based passive radar sensors," *IEEE Sensors J.*, vol. 17, no. 15, pp. 4757–4772, Aug. 2017.

[13] A. Zaimbashi, "Target detection in analog terrestrial TV-based passive radar sensor: Joint delay-Doppler estimation," *IEEE Sensors J.*, vol. 17, no. 17, pp. 5569–5580, Sep. 2017.

[14] P. Stinco, M. S. Greco, F. Gini, and M. Rangaswamy, "Ambiguity function and Cramér—Rao bounds for universal mobile telecommunications system-based passive coherent location systems," *IET Radar Sonar Navigat.*, vol. 6, no. 7, pp. 668–678, Aug. 2012.

[15] S. Gogineni, M. Rangaswamy, B. D. Rigling, and A. Nehorai, "Cramér—Rao bounds for UMTS-based passive multistatic radar," *IEEE Trans. Signal Process.*, vol. 62, no. 1, pp. 95–106, Jan. 2014.

[16] M. N. Javed, S. Ali, and S. A. Hassan, "3D MCRLB evaluation of a UMTS-based passive multistatic radar operating in a line-of-sight environment," *IEEE Trans. Signal Process.*, vol. 64, no. 19, pp. 5131–5144, Oct. 2016.

[17] V. Anastasio, A. Farina, F. Colone, and P. Lombardo, "Cramér—Rao lower bound with P d < 1 for target localisation accuracy in multistatic passive radar," *IET Radar, Sonar Navigat.*, vol. 8, no. 7, pp. 767–775, Aug. 2014.

[18] Q. He and R. S. Blum, "The significant gains from optimally processed multiple signals of opportunity and multiple receive stations in passive radar," *IEEE Signal Process. Lett.*, vol. 21, no. 2, pp. 180–184, Feb. 2014.

[19] C. Shi, F. Wang, and J. Zhou, "Cramér—Rao bound analysis for joint target location and velocity estimation in frequency modulation based passive radar networks," *IET Signal Process.*, vol. 10, no. 7, pp. 780–790, Sep. 2016.

[20] C. Shi, F. Wang, M. Sellathurai, and J. Zhou, "Transmitter subset selection in FM-based passive radar networks for joint target parameter estimation," *IEEE Sensors J.*, vol. 16, no. 15, pp. 6043–6052, Aug. 2016.

[21] F. D. V. Maasdorp, R. Nadjiasngar, and M. R. Inggs, "A Cramér—Rao analysis on receiver placement in a FM band Commensal Radar system based on Doppler only measurements," in *Proc. Int. Radar Conf.*, Oct. 2014, pp. 1–6.

[22] P. Stinco, M. Greco, F. Gini, and A. Farina, "Sensor selection in PCL radar systems based on bistatic PCRLB," in *Proc. Workshop Adv. Radar Remote Sens. (TyWRRS)*, Sep. 2012, pp. 41–45.

[23] Q. He, J. Hu, R. S. Blum, and Y. Wu, "Generalized Cramér—Rao bound for joint estimation of target position and velocity for active and passive radar networks," *IEEE Trans. Signal Process.*, vol. 64, no. 8, pp. 2078–2089, Apr. 2016.

[24] X. Zhang, H. Li, J. Liu, and B. Himed, "Joint delay and Doppler estimation for passive sensing with direct-path interference," *IEEE Trans. Signal Process.*, vol. 64, no. 3, pp. 630–640, Feb. 2016.

[25] Y. Zhao, Y. Zhao, and C. Zhao, "Joint delay—Doppler estimation for passive bistatic radar with direct-path interference using MCMC method," *IET Radar Sonar Navigat.*, vol. 12, no. 1, pp. 130–136, Oct. 2017.

[26] J. Hu, Q. He, R. S. Blum, and Y. Wu, "Performance analysis of joint parameter estimation for distributed radar networks under a general model," in *Proc. IET Int. Radar Conf.*, Oct. 2015, pp. 1–5.

[27] X. Zhang, H. Li, and B. Himed, "Multistatic passive detection in the presence of direct-path interference," in *Proc. IEEE Radar Conf. (RadarConf)*, Seattle, WA, USA, May 2017, pp. 524–529.

[28] G. Cui, J. Liu, H. Li, and B. Himed, "Target detection for passive radar with noisy reference channel," in *Proc. IEEE Radar Conf.*, Cincinnati, OH, USA, May 2014, pp. 144–148.

[29] F. Wang, H. Li, X. Zhang, and B. Himed, "Signal parameter estimation for passive bistatic radar with waveform correlation exploitation," *IEEE Trans. Aerosp. Electron. Syst.*, vol. 54, no. 3, pp. 1135–1150, Jun. 2018.

[30] G. Cui, J. Liu, H. Li, and B. Himed, "Signal detection with noisy reference for passive sensing," *Signal Process.*, vol. 108, pp. 389–399, Mar. 2015.

[31] D. E. Hack, L. K. Patton, B. Himed, and M. A. Saville, "Centralized passive MIMO radar detection without direct-path reference signals," *IEEE Trans. Signal Process.*, vol. 62, no. 11, pp. 3013–3023, Jun. 2014.

[32] D. E. Hack, L. K. Patton, B. Himed, and M. A. Saville, "Detection in passive MIMO radar networks," *IEEE Trans. Signal Process.*, vol. 62, no. 11, pp. 2999–3012, Jun. 2014.

[33] A. Nehorai and P. Stoica, "Adaptive algorithms for constrained ARMA signals in the presence of noise," *IEEE Trans. Acoust., Speech, Signal Process.*, vol. 36, no. 8, pp. 1282–1291, Aug. 1988.

[34] H. Tong, "Autoregressive model fitting with noisy data by Akaike's information criterion," *IEEE Trans. Inf. Theory*, vol. 21, no. 4, pp. 476–480, Jul. 1975.
[35] H. Fan, T. Soderstrom, and Y. Zou, "Continuous-time AR process parameter estimation in presence of additive white noise," *IEEE Trans. Signal Process.*, vol. 47, no. 12, pp. 3392–3398, Dec. 1999.

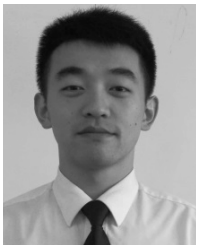

JING TONG was born in Liaoning, China, in 1995. He received the B.S. degrees in information countermeasure from the Naval University of Engineering, Wuhan, Hubei, in 2017, where he is currently pursuing the Ph.D. degree in communication and information system. His research interests include passive detection, passive coherent location, and signal processing.

HUANG GAOMING was born in Hunan, China, in 1972. He received the B.S. and M.E. degrees in electronic warfare from the Naval Electronic College of Engineering, China, in 1995 and 1998, respectively, and the Ph.D. degree in signal processing from Dongnan University, Nanjing, China, in 2006. He is currently the Chief Professor with the Department of Information Countermeasure, Naval University of Engineering, China. His research interests include passive detection, intelligent signal processing, and electronic warfare system simulation.

TIAN WEI was born in Hebei, China, in 1984. He received the B.E. degree in communication engineering from Harbin Engineering University, China, in 2007, and the Ph.D. degree in information and communication engineering from Tsinghua University, China, in 2014. He holds a postdoctortoral position at the College of Electronic Engineering, Naval University of Engineering, China. His research interests include information fusion, radar signal processing, and radar electronic warfare.

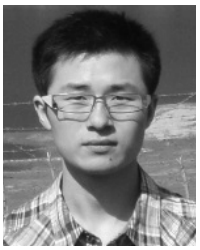

PENG HUAFU was born in Hubei, China, in 1987. He received the B.S. degree in electronic engineering and the M.S. degree in information and communication engineering from Information Engineering University, Zhengzhou, Henan, in 2008 and 2013, respectively. He is currently pursuing the Ph.D. degree in mechanical engineering with the Naval University of Engineering, China. His research interests include information fusion and communication signal processing.